A NUMERICAL STUDY FOR THE PERFORMANCE OF THE RUNGE-KUTTA FINITE DIFFERENCE METHOD BASED ON DIFFERENT NUMERICAL HAMILTONIANS

HASEENA AHMED AND HAILIANG LIU

Abstract. High resolution finite difference methods have been successfully employed in solving Hamilton Jacobi equations, and numerical Hamiltonians are as important as numerical fluxes for solving hyperbolic conservation laws using the finite volume methodology. Though different numerical Hamiltonians have been suggested in the literature, only some simple ones such as the Lax-Friedrichs Hamiltonian are widely used. In this paper, we identify six Hamiltonians and investigate the performance of Runge-Kutta ENO methods introduced by Shu and Osher in [*SIAM J. Numer. Anal. (28)(4):907-922, 1991*] based on different numerical Hamiltonians, with the objective of obtaining better performance by selecting suitable numerical Hamiltonians. Extensive one dimensional numerical tests indicate that Hamiltonians with the upwinding property perform the best when factors such as accuracy and resolution of kinks are addressed. However, when the order of accuracy of the scheme and the number of grid points are increased, the errors for all Hamiltonians become nearly equal. Numerical tests are also performed for two dimensional problems.

Contents

1. Introduction

In this paper, we investigate the performance of the Runge-Kutta finite difference (RKFD) method with essentially non-oscillatory (ENO) approximation [11, 24, 13, 10, 27, 28, 25, 26] based on different numerical Hamiltonians for solving the Hamilton Jacobi (HJ) equation

$$\begin{cases} \partial_t \phi + H(D\phi) = 0 \quad \text{in} \quad \mathbb{R}^n \times (0,\infty), \\ \phi = \phi_0 \quad \text{in} \quad \mathbb{R}^n \times \{t=0\}, \end{cases} \tag{1.1}$$

with the objective of obtaining better performance by choosing suitable numerical Hamiltonians.

The Hamilton-Jacobi equation arises in many applications such as geometrical optics, crystal growth, computer vision, and geometric motion. From method of characteristics

[7], we know that in general there can be no smooth solution of (1.1) lasting for all times $t \geq 0$. These problems have been approached by Crandall and Lions in 1983 [3] by introducing the notion of viscosity. Evans [7] gives the motivation to the formulation of viscosity solutions from maximum principle; existence and uniqueness is proved in the paper [3]. The viscosity solutions of HJ equations are Lipschitz continuous but with discontinuous derivatives even if the Hamiltonian H and the initial condition $\phi_0(x)$ is C^∞. We mention in passing that in some other applications such as high frequency wave propagation problems viscosity solutions are not adequate in describing the physical behavior beyond the singularity, and multi-valued solutions have to be considered, see e.g. [6, 21] for recent accounts of numerical methods developed in computation of multi-valued solutions.

We now illustrate roles of numerical Hamiltonians for 1D case. The numerical method for multi-D HJ equation can be constructed in a dimension by dimension fashion. A forward Euler in time discretization for 1D HJ equation gives

$$\frac{\phi^{n+1}-\phi^n}{\Delta t} + \hat{H}^n(\phi_x^-, \phi_x^+) = 0,$$

where $\hat{H}(\phi_x^-, \phi_x^+)$ is a numerical approximation of H, and it is required to be consistent in the sense that $\hat{H}(\phi_x, \phi_x) = H(\phi_x)$. The spatial derivatives such as ϕ_x^- and ϕ_x^+ are discretized simply with first order accurate one-sided differencing. The choice of monotone Hamiltonians leads to an important class of numerical methods for solving (1.1) which is the class of monotone schemes discussed by Crandall and Lions [4]. Here the monotonicity of the scheme means that ϕ^{n+1} as defined by the scheme is a nondecreasing function of all the ϕ^n. Crandall and Lions proved that monotone schemes are convergent to the viscosity solution, although they are only first order accurate.

Following this framework, we shall construct numerical methods by discretizing the approximate equation of the form

$$\partial_t \phi + \hat{H}(\phi_x^-, \phi_x^+) = 0, \tag{1.2}$$

where $\hat{H}$ is an approximation of H. Here $\phi_x^- = \phi_x(x-0,t)$ and $\phi_x^+ = \phi_x(x+0,t)$ denote the left and right limits of ϕ_x crossing the discontinuity. The approximate equation (1.2) is equivalent to the original equation for smooth solutions, and for solutions with discontinuous derivatives the approximate Hamiltonian $\hat{H}$ needs to be selected so that the right solution–viscosity solution–can be singled out.

All terms in equation (1.2) are now well defined for functions of Lipschitz continuity in spatial variables, then the algorithm for solving it with the same initial data $\phi_0(x)$ becomes standard. We define point values

$$\phi(t) = \{\phi_j(t) = \phi(x_j, t)\}, \quad t > 0,$$

and then construct a continuous piecewise polynomial of the form

$$\tilde{\phi}(x, t_n) = P^{\phi(t)}_{j+\frac{1}{2}}(x), \quad x \in [x_j, x_{j+1}].$$

Evaluation of (1.2) at $x = x_j$ gives

$$\frac{d}{dt}\phi_j(t) = -\hat{H}((\phi_x^-)_j, (\phi_x^+)_j), \tag{1.3}$$

where

$$(\phi_x^+)_j = \partial_x P^{\phi(t)}_{j+\frac{1}{2}}(x_j), \quad (\phi_x^-)_j = \partial_x P^{\phi(t)}_{j-\frac{1}{2}}(x_j).$$

We then solve the semi-discrete system (1.3) by a high-order discretization in time. In this paper we follow [24] by using the ENO approximation for spatial reconstruction, and TVD Runge-Kutta [8, 9] to achieve higher order time discretization. Though other high resolution numerical methods can be employed for discretizing the approximate equation (1.2) as well.

An important component for making the above algorithm to work is the numerical Hamiltonian, which corresponds to the numerical flux for solving hyperbolic conservation laws using the finite volume methodology. In past decades, various high resolution numerical methods have been proposed for solving Hamilton Jacobi equations, and essentially they differ in either the way of spatial reconstruction or the choice of numerical Hamiltonians. Some Hamiltonians are motivated from the numerical flux for conservation laws [12, 5, 29], and others are based on derivation using staggered central approximation [20, 17, 1, 2, 18]. We note that many existing reconstruction procedures for high order finite difference schemes must involve wide stencils, thus the numerical result with refined meshes may not seem sensitive to the choice of Hamiltonians. However, for higher-order approximations constructed within each computational cell such as in the discontinuous Galerkin methods [14, 19], the numerical Hamiltonian becomes more important in its role communicating with immediate cell neighbors.

The goal of this paper is to identity six popular Hamiltonians and compare the numerical performance of well-developed Runge-Kutta ENO methods based on different numerical Hamiltonians, with the objective of obtaining better performance by choosing a suitable numerical Hamiltonian. All the numerical Hamiltonians $\hat{H}$ presented are locally Lipschitz continuous, consistent with H and monotone. Another favorable feature is upwinding. The term upwinding refers to the fact that spatial differencing is performed using mesh points on the side from which information flows. The mathematical formulation for these terminologies is given in Section 2. Among six Hamiltonians presented within this work, the Lax-Friedrich's and Central Hamiltonian are not upwinding, but the Godunov, Engquist-Osher, Harten-Lax-van Leer and the Roe Hamiltonian are all upwinding.

For high order spatial discretization, essentially non-oscillatory(ENO) schemes (Harten and Osher [13], Harten, Engquist, Osher and Chakravarthy [11], Shu and Osher [27, 28]) have been very successful in solving hyperbolic conservation laws. The key idea of ENO approximation is the adaptive stencil procedure which automatically obtains information from the locally smoothest region, and hence yields a uniformly high-order essentially non-oscillatory approximation for piecewise smooth functions. Weighted ENO (WENO) schemes were developed for conservation laws using convex combination of all candidate stencils instead of just one as in the original ENO [22, 16]. ENO and WENO schemes for Hamilton-Jacobi type equations were designed in [24, 15].

The plan of this paper is as follows: In Section 2 we introduce a notion of upwind-type Hamiltonian, and give the description of six numerical Hamiltonians under consideration. In Section 3 we review the ENO reconstruction procedure and the Runge-Kutta time discretization, as adapted from the work by Shu and Osher [24]. In Section 4, we present extensive numerical experiments in one-dimension case and some tests in two-dimensional case to compare the performance. Concluding remarks are given in Section 5.

2. Effective Numerical Hamiltonians

In order for the approximation equation (1.2) to be faithful to the original Hamilton Jacobi equation, the numerical Hamiltonian has to be carefully chosen. An ideal Hamiltonian should satisfy the following requirements.

Definition: A Hamiltonian $\hat{H}$ is said to be an upwind-type Hamiltonian if

(i)(Consistency) $\hat{H}(u,u) = H(u)$

(ii)(Monotonicity) $\hat{H}(u^-,u^+)$ is nondecreasing in u^- and non-increasing in u^+.

(ii)(Upwind) $\hat{H}(u^-,u^+) = H(u^+)$ when $H_u < 0$ for all u between u^+ and u^-; $\hat{H}(u^-,u^+) = H(u^-)$ when all $H_u > 0$.

The monotonicity is required to ensure the entropy stability, but may lead to excessive dissipation. The characteristics imposed by the upwind requirement is expected to help sharpen things up again.

In this section we present different numerical Hamiltonians used in the comparison study for 1-D and 2-D case for the RKFD method. Extensive numerical experiments to compare their performance for this method is given in Section 4. First, we review six numerical Hamiltonians under consideration for the 1-D case. Notation $I(a,b)$ is used to denote the interval $[\min(u^+,u^-), \max(u^+,u^-)]$.

1. **Lax-Friedrich's (LF) Hamiltonian and the local LF (LLF) Hamiltonian**: The LF Hamiltonian is one of the simplest and most widely used numerical Hamiltonian for the ENO method. However, the numerical viscosity of the LF Hamiltonian is also the largest among monotone Hamiltonians for scalar problems. It is defined as

$$\hat{H}^{LF}(u^+,u^-) = H\left(\frac{u^+ + u^-}{2}\right) - \sigma(u^+,u^-)\left(\frac{u^+ - u^-}{2}\right),$$

where for the LF Hamiltonian, we obtain a bound for the maximal speed of propagation as

$$\sigma = \max_{u\in[A,B]} |H'(u)|,$$

where $[A,B]$ is the range of u. For a LLF Hamiltonian we have from [24] that

$$\sigma_i = \max_{u\in I(u_i^+,u_i^-)} |H'(u)|.$$

For convex Hamiltonian, σ_i is given as $\max\left\{|H'(u_i^+)|, |H'(u_i^-)|\right\}$. Clearly the LF Hamiltonian is not upwinding.

2. **Central Hamiltonian**: Recently, high resolution central type schemes having non-oscillatory property have been introduced for Hamilton-Jacobi equations by Lin and Tadmor [20], followed by [17, 1, 2, 18]. The idea presented in [18] involves a two step process - evolution and projection. Given solution values ϕ_i at the grid points x_i, we evolve in time the values of ϕ at the point $x_{i\pm}^n := x_i + \sigma_i^n \Delta t$, where σ_i^n is the maximum speed of propagation. The evolution is given by a Taylor series expansion as follows:

$$\phi_{i\pm}^{n+1} = \tilde{\phi}(x_{i\pm}, t^n) - \Delta t H(\tilde{\phi}_x(x_{i\pm}^n, t^n)),$$

where $\tilde{\phi}$ is the reconstructed piecewise polynomial interpolant, and $\tilde{\phi}_x$ its derivative. The solution is then projected back to the original grid points x_i, $i = 0, 1, 2, \ldots$, by using the average $\phi_i^{n+1} = \frac{1}{2}(\phi_{i+}^{n+1} + \phi_{i-}^{n+1})$. The resulting scheme has a semi-discrete form

$$\frac{d}{dt}\phi(t) = -\frac{1}{2}\left(H(\phi_x^+(t)) + H(\phi_x^-(t))\right) + \sigma_i(t)\left(\frac{\phi_x^+(t) - \phi_x^-(t)}{2}\right). \tag{2.1}$$

A $k-$th order scheme is obtained by using a $k-$th order polynomial interpolant for $\tilde{\phi}$ and $k-$th order Taylor expansion in time. Using our notation for high order forward and backward difference approximations for the derivative ϕ_x as u^+ and u^-, we can write the Central Hamiltonian from equation (2.1) as

$$\hat{H}^{Central}(u^+, u^-) = \frac{1}{2}\left(H(u^+) + H(u^-)\right) - \sigma(u^+, u^-)\left(\frac{u^+ - u^-}{2}\right).$$

The maximum speed of propagation σ is calculated as in the case of the LLF Hamiltonian.

3. **Godunov's Hamiltonian**: The Godunov Hamiltonian is obtained by attempting to solve the Riemann problem of the equation (1.1) exactly with piecewise linear initial condition determined by $u^{\pm}$. It can be given in its closed form as [24]

$$\hat{H}^{God}(u^+, u^-) = \begin{cases} \min\limits_{u^- \le u \le u^+} H(u) & \text{if } u^- \le u^+, \\ \max\limits_{u^+ \le u \le u^-} H(u) & \text{if } u^- > u^+. \end{cases}$$

The Godunov Hamiltonian is purely upwind and is the least dissipative among all monotone Hamiltonians [23], but could be very costly to evaluate in the 2-D case, as it often lacks explicit formulas and relies on iterative procedures for its evaluation.

4. **Engquist-Osher Hamiltonian**: The Engquist-Osher flux was originally defined for hyperbolic conservation laws by using the flux splitting technique in [5], details of which could be found in [29]. We propose a numerical Hamiltonian of a similar nature as follows

$$\hat{H}^{EO}(u^+, u^-) = \frac{1}{2}\left(H(u^+) + H(u^-) - \int_{u^-}^{u^+} |H'(u)|\, du\right).$$

The integral in the EO Hamiltonian can be calculated exactly most times for scalar Hamiltonians.

5. **Harten-Lax-van Leer(HLL) Hamiltonian**: The HLL flux was first introduced for hyperbolic conservation laws in [12] by Harten, Lax and van Leer by using approximate Riemann solvers. In the context of Hamilton Jacobi equations, the corresponding Hamiltonian can be written as

$$\hat{H}^{HLL}(u^+, u^-) = \frac{a_j^- H(u^+) + a_j^+ H(u^-)}{a_j^+ + a_j^-} - \frac{a_j^+ a_j^-}{a_j^+ + a_j^-}\left(u^+ - u^-\right).$$

For every grid point, the maximal right and left speeds of propagation a_j^+ and a_j^- are estimated by

$$\begin{aligned} a_j^+ &= \max_{u\in I(u^+,u^-)} \{H'(u), 0\}, \\ a_j^- &= |\min_{u\in I(u^+,u^-)} \{H'(u), 0\}|. \end{aligned}$$

For convex Hamiltonians, this reduces to

$$\begin{aligned} a_j^+ &= \max\left\{H'(u^+), H'(u^-), 0\right\}, \\ a_j^- &= |\min\left\{H'(u^+), H'(u^-), 0\right\}|. \end{aligned}$$

Note that the above Hamiltonian was recently derived for Hamilton Jacobi equations by Bryson, Kurganov, Levy and Petrova in [1].

6. **Roe with Local Lax Friedrich fix Hamiltonian**: Here upwinding idea is used in the construction of the Hamiltonian. The Roe Hamiltonian is defined in [24] as follows:

$$\hat{H}^{Roe}(u^+,u^-) = \begin{cases} H(u^*) & \text{if } H'(u) \text{ does not change sign in the} \\ & \text{region } u \in I(u^+,u^-), \\ \hat{H}^{LLF} & \text{otherwise,} \end{cases}$$

where u^* is defined from upwinding as,

$$u^* = \begin{cases} u^+ & \text{if } H'(u) \le 0, \\ u^- & \text{if } H'(u) \ge 0. \end{cases}$$

$\hat{H}^{Roe}$ has almost as small dissipation as $\hat{H}^{God}$.

For the 2-D case, u^+ and u^- are used to denote the high order approximations to the derivative along the x-direction, that is ϕ_x^+ and ϕ_x^- and v^+ and v^- are used to denote that along the y-direction ϕ_y^+ and ϕ_y^-. The numerical Hamiltonians for 2-D systems are each functions of u^+, u^-, v^+ and v^- and can be given as follows:

1. **Lax-Friedrich's (LF) Hamiltonian and the local LF (LLF) Hamiltonian**: It is defined by [24]

$$\begin{aligned} \hat{H}^{LF} &= H\left(\frac{u^+ + u^-}{2}, \frac{v^+ + v^-}{2}\right) - \sigma_x(u^+,u^-)\left(\frac{u^+ - u^-}{2}\right) \\ &\quad -\sigma_y(v^+,v^-)\left(\frac{v^+ - v^-}{2}\right), \end{aligned}$$

where for the LF Hamiltonian, we have the maximum speeds of propagation in the x and y direction given by

$$\sigma_x = \max_{\substack{u\in[A,B]\\ v\in[C,D]}} |H_u(u,v)|, \qquad \sigma_y = \max_{\substack{u\in[A,B]\\ v\in[C,D]}} |H_v(u,v)|,$$

where $[A, B]$ is the range of u and $[C, D]$ is the range of v. For a LLF Hamiltonian we have that

$$\sigma_x = \max_{\substack{u\in I(u^-,u^+)\\ v\in[C,D]}} |H_u(u,v)|, \qquad \sigma_y = \max_{\substack{v\in I(v^-,v^+)\\ u\in[A,B]}} |H_v(u,v)|.$$

2. **Central Hamiltonian**: High resolution central schemes having non-oscillatory property are derived for 2-D systems in the same way as the 1-D system [18]. We can write the Central Hamiltonian as

$$\begin{aligned}\hat{H}^{Central} &= \frac{1}{4}\left[H(u^+,v^+)+H(u^+,v^-)+H(u^-,v^+)+H(u^-,v^-)\right]\\ &\quad -\sigma(u^+,u^-,v^+,v^-)\left(\frac{u^+-u^-+v^+-v^-}{2}\right),\end{aligned}$$

where the maximal local speed of propagation $\sigma_{j,k}$ is given by the maximal value over the square $C_{j,k} := \left\{(x,y)\in[x_{j-\frac{1}{2}}, x_{j+\frac{1}{2}}]\times[y_{j-\frac{1}{2}}, y_{j+\frac{1}{2}}]\right\}$

$$\sigma^n_{j,k} = \max_{C_{j,k}}\{|H_u(u,v)|, |H_v(u,v)|\}$$

3. **Harten-Lax-van Leer(HLL) Hamiltonian**: The HLL Hamiltonian for 2-D Hamilton Jacobi equations was derived by Bryson, Kurganov, Levy and Petrova in [1] and is given by

$$\begin{aligned}\hat{H}^{HLL} &= \frac{a^-b^-H(u^+,v^+)+a^-b^+H(u^+,v^-)+a^+b^-H(u^-,v^+)+a^+b^+H(u^-,v^-)}{(a^++a^-)(b^++b^-)}\\ &\quad -\frac{a^+a^-}{a^++a^-}\left(u^+-u^-\right)-\frac{b^+b^-}{b^++b^-}\left(v^+-v^-\right).\end{aligned}$$

For every grid point (x_j, y_k), the maximal right and left speeds of propagation in the x direction, a^+_{jk} and a^-_{jk} and in the y direction, b^+_{jk} and b^-_{jk} are estimated by

$$\begin{aligned}a^+_{jk} &= \max_{C_{j,k}}\{H_u(u,v),0\}, \qquad a^-_{jk} = |\min_{C_{j,k}}\{H_u(u,v),0\}|,\\ b^+_{jk} &= \max_{C_{j,k}}\{H_v(u,v),0\}, \qquad b^-_{jk} = |\min_{C_{j,k}}\{H_v(u,v),0\}|,\end{aligned}$$

where the square $C_{j,k}$ is given as in the 2-D Central Hamiltonian.

4. **Roe with Local Lax Friedrich fix Hamiltonian**: It is defined in [24] as follows:

$$\hat{H}^{Roe} = \begin{cases} H(u^*,v^*), \\ \quad \text{if } H_u \text{ and } H_v \text{ do not change sign in } u\in I(u^-,u^+), v\in I(v^-,v^+), \\ H\left(\frac{u^++u^-}{2}, v^*\right)-\sigma_x\left(\frac{u^+-u^-}{2}\right), \\ \quad \text{otherwise if } H_v \text{ does not change sign in } u\in[A,B], v\in I(v^-,v^+), \\ H\left(u^*, \frac{v^++v^-}{2}\right)-\sigma_y\left(\frac{v^+-v^-}{2}\right), \\ \quad \text{otherwise if } H_u \text{ does not change sign in } u\in I(u^-,u^+), v\in[C,D], \\ \hat{H}^{LLF}(u^+,u^-,v^+,v^-), \\ \quad \text{otherwise,}\end{cases}$$

where σ_x and σ_y are given as in LLF Hamiltonian, u^* and v^* are defined purely by upwinding as

$$u^* = \begin{cases} u^+ & \text{if } H_u(u,v) \le 0, \\ u^- & \text{if } H_u(u,v) \ge 0, \end{cases}$$

$$v^* = \begin{cases} v^+ & \text{if } H_v(u,v) \le 0, \\ v^- & \text{if } H_v(u,v) \ge 0. \end{cases}$$

3. High-resolution discretization

In this section, we give a brief description of the RKFD method with ENO approximation for the one dimensional case. We use notations in [25].

We wish to solve the one-dimensional Hamilton Jacobi equation

$$\begin{cases} \phi_t + H(\phi_x) = 0 & \text{in} \quad [a,b]\times(0,\infty), \\ \phi = \phi_0 & \text{in} \quad [a,b]\times\{t=0\}. \end{cases} \tag{3.1}$$

The computational domain $[a,b]$ is divided into n cells $a = x_0 < x_1 < \ldots < x_{n-1} < x_n = b$. We assume a uniform grid in space and time with grid spacing Δx and Δt, respectively. The grid points are denoted by $x_i := i\Delta x, t^n := n\Delta t$, and the approximate value of $\phi(x_i,t^n)$ is denoted by ϕ_i^n. The numerical approximation to the viscosity solution $\phi(x_i,t^n)$ of (3.1) at the mesh point (x_i,t^n) is denoted by ϕ_i^n. We use finite difference methods to calculate ϕ_i^n for which the derivatives occurring in (3.1) are replaced by appropriate finite difference approximations. Since the solutions to Hamilton Jacobi equations have discontinuous derivatives ϕ_x, we consider that the left and right hand limits of the discontinuous derivative of the solution ϕ_x^- and ϕ_x^+ exist at the cell interface x_i and define a numerical Hamiltonian $\hat{H}$ as a function of these.

If we use the notations $\phi_{x_i^+} = \frac{\phi_{i+1}-\phi_i}{\Delta x}$ and $\phi_{x_i^-} = \frac{\phi_i-\phi_{i-1}}{\Delta x}$ to denote the first order forward and backward difference approximations to the right and left derivatives of $\phi(x)$ at the location x_i. A first order monotone finite difference scheme for (3.1) can be given as

$$\phi_i^{n+1} = \phi_i^n - \Delta t\hat{H}(\phi^n_{x_i^+}, \phi^n_{x_i^-}). \tag{3.2}$$

The ENO interpolation idea is used to obtain higher order approximations to the derivative $\phi_x^{\pm}$. The key feature of the ENO algorithm is an adaptive stencil high order interpolation which tries to avoid shocks or high gradient regions whenever possible and hence works well with Hamilton-Jacobi equations. If u_i^+ and u_i^- denote high order approximations to the derivative ϕ_x^+ and ϕ_x^-, the finite difference approximation

$$\phi_i^{n+1} = \phi_i^n - \Delta t\hat{H}(u^+(t), u^-(t)), \tag{3.3}$$

gives a higher order finite difference scheme in space. The key feature of ENO to avoid numerical oscillations in the solution of Hamilton-Jacobi equations is through the interpolation procedure to obtain $u_i^{\pm}$.

Given point values $f(x_i)$, $i = 0, \pm1, \pm2, \ldots$ of a (usually piecewise smooth) function $f(x)$ at discrete nodes x_i , we associate an $r-$th degree polynomial $P^{f,r}_{i+\frac{1}{2}}(x)$ with each interval $[x_i, x_{i+1}]$, with the left-most point in the stencil as $x_{k^{(r)}_{min}}$, constructed inductively by the algorithm from [24]:

1. $P^{f,1}_{i+\frac{1}{2}}(x) = f[x_i] + f[x_i, x_{i+1}](x - x_i), k^{(1)}_{min} = i;$

2. If $k_{min}^{(l-1)}$ and $P_{i+\frac{1}{2}}^{f,l-1}(x)$ are both defined, then let

$$\begin{aligned} a^{(l)} &= f[x_{k_{min}^{(l-1)}}, \ldots, x_{k_{min}^{(l-1)}+l}], \\ b^{(l)} &= f[x_{k_{min}^{(l-1)}-1}, \ldots, x_{k_{min}^{(l-1)}+l-1}], \text{ and} \end{aligned}$$

i. if $|a^{(l)}| \geq |b^{(l)}|$, then $c^{(l)} = b^{(l)}$ and $k_{min}^{(l)} = k_{min}^{(l-1)} - 1$; otherwise $c^{(l)} = a^{(l)}$ and $k_{min}^{(l)} = k_{min}^{(l-1)}$;

ii. $P_{i+\frac{1}{2}}^{f,l}(x) = P_{i+\frac{1}{2}}^{f,l-1}(x) + c^{(l)} \prod_{i=k_{min}^{(l-1)}}^{k_{min}^{(l-1)}+l-1} (x - x_i)$.

The approximations to the left and right $x-$derivatives of ϕ are then taken as

$$u_i^{\pm} = \frac{\partial}{\partial x} P_{i+\frac{1}{2}}^{\phi,r}(x_i).$$

Here $f[\ldots]$ denote Newton divided differences.

For high order accuracy in time, a high order TVD Runge-Kutta time discretization [8, 9] is used. Time step restriction is taken as

$$\frac{\Delta t}{\Delta x} \max_u \left| \frac{\partial}{\partial u} H(u) \right| \leq 0.3,$$

where the maximum is taken over the relevant ranges of u. Here 0.3 is just a convenient number used. Also, since the higher order interpolation for derivatives can be extended dimension by dimension, it is easy to implement ENO approximation scheme for higher dimensions as well.

4. Numerical Test

In this section, we perform extensive numerical experiments to compare the performance of the ENO approximation method based on the six different Hamiltonians outlined in the previous section. The detailed numerical study is performed mainly for the one dimensional case addressing issues of CPU cost, accuracy, non-oscillatory property, and resolution of discontinuities. Numerical tests are also performed for 2-dimensional case. In all the figures, we plot the point values of the numerical solution at the grid points. For CPU time comparison, all the computations are performed on a Dell Digital personal workstation, Intel Pentium 4 CPU, 2GHz, 1GB RAM. In our numerical experiments, the CFL number is taken as 0.3 for the first, second and third order accuracy. In all the three one-dimensional examples, the reference "exact" solution is computed using a fifth order WENO [16, 26] and fourth order TVD Runge-Kutta [9, 8] using 10240 cells.

We denote the finite difference method with ENO interpolation and Hamiltonian "X" as ENO-X, such as ENO-LLF for the RKFD scheme with LLF Hamiltonian. In comparing the L^1 and L^∞ errors we use notation "ENO-X $\gg$ ENO-Y" (or "ENO-X $\approx$ ENO-Y") to indicate that error from using Hamiltonian X is greater than (or equal to the order of 10^{-15}) that while using Hamiltonian Y.

Example 4.1. We work with an example in [24] which is a standard test problem for Hamilton-Jacobi equations. Consider, a 1-dimensional equation given by

$$\begin{aligned} \phi_t + \frac{(\phi_x + 1)^2}{2} &= 0, \qquad -1 \le x \le 1, \\ \phi(x, 0) &= -\cos \pi x. \end{aligned}$$

Here, the Hamiltonian is a convex function and we can use the simplified expressions given in the previous section for the computation of the maximal speed of propagation.

We use periodic boundary conditions and compute the solution and test accuracy when it is smooth, that is, up to time $T = \frac{0.5}{\pi^2}$. Since the LLF Hamiltonian is widely used, we use it as a reference to analyze the performance of other Hamiltonians. In Table 1, we provide a CPU time comparison for the RKFD scheme with different Hamiltonians. Note that this CPU time comparison depends on our specific implementation of these Hamiltonians and also on the specific test case. The numerical errors and the orders of accuracy for the numerical solution ϕ_i^n, and ratios of the numerical errors for comparison with the ENO-LLF scheme are shown in Tables 2-4.

All the schemes give the desired accuracy in space. The L^1 error depends on the order of ENO approximation and the number of cells used. For first order scheme, ENO-Central gives the largest and ENO-God gives the smallest L_1 and L^∞ errors among all the schemes. From Table 2, we can see that for small number of cells ($N = 20, 40$), the L^1 error by ENO-God, ENO-EO, ENO-HLL and ENO-Roe are about $80 - 90\%$ of the L^1 error by ENO-LLF and as the number of cells increase ($N \ge 80$), the error by ENO-God, ENO-EO, ENO-HLL and ENO-Roe are about $94 - 98\%$ of the L^1 error by ENO-LLF. For the second and third order schemes, we can see from Tables 3 and 4 that for small number of cells ENO-Central gives the largest and ENO-God gives the smallest L_1 error, but as the number of cells is increased, the errors become very close to each other.

The main difference comes into play in the computation time. The total CPU time for $N = 20, 40, 80, 160, 320, 640$ and 1280 cells is recorded in Table 1. The ENO-Central and the ENO-EO Hamiltonians take about nearly the same computation time as of the ENO-LLF scheme. ENO-God takes about 70 times the time taken by ENO-LLF for the first order scheme, about 55 times the time taken by ENO-LLF for the second order scheme and about 45 times the time taken by ENO-LLF for the third order scheme. ENO-HLL takes about 20% more time than the ENO-LLF, and ENO-Roe takes about $3 - 5$ times the time taken by ENO-LLF for 1st, 2nd and 3rd order schemes.

Table 1: Total CPU time in seconds for the RKFD method with ENO approximation with different Hamiltonians. The sum of the CPU times for $N = 20, 40, 80, 160, 320, 640$ and 1280 cells is recorded for Example 4.1 for orders 1, 2, and 3.

Order	LLF	Central	God	EO	HLL	Roe
1	1.06	1.06	73.11	1.05	1.20	4.72
2	2.64	2.61	141.19	2.92	3.22	10.08
3	4.61	4.34	214.83	4.80	5.59	15.94

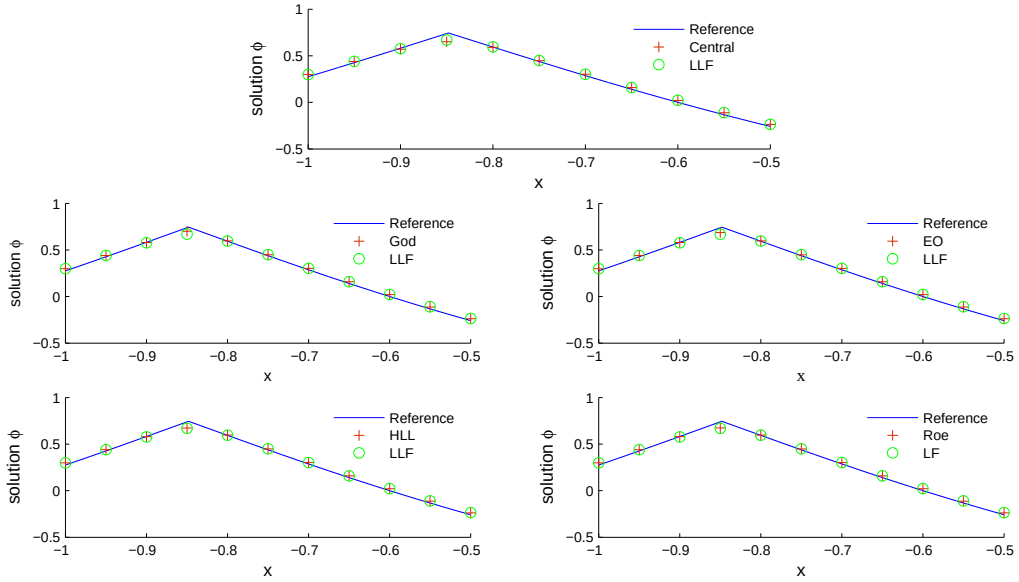

Figure 1: Resolution of discontinuities for example 4.1, 1**st order**, at $T = \frac{1.5}{\pi^2}$, 40 cells, zoomed at the region $-1 \leq x \leq -0.5$ which contains the discontinuous derivative.

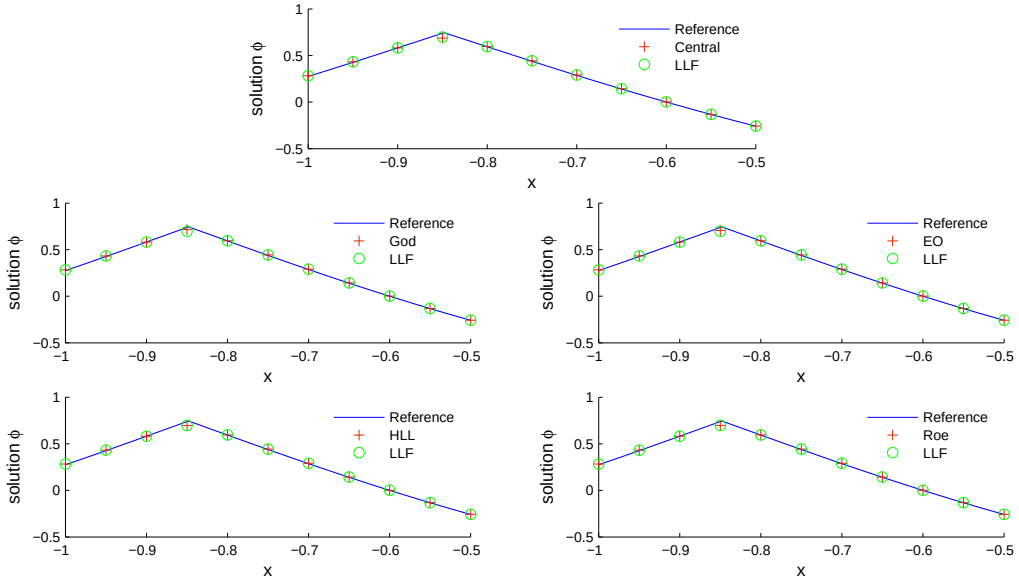

Figure 2: Resolution of discontinuities for example 4.1, 2**nd order**, at $T = \frac{1.5}{\pi^2}$, 40 cells, zoomed at the region $-1 \leq x \leq -0.5$ which contains the discontinuous derivative.

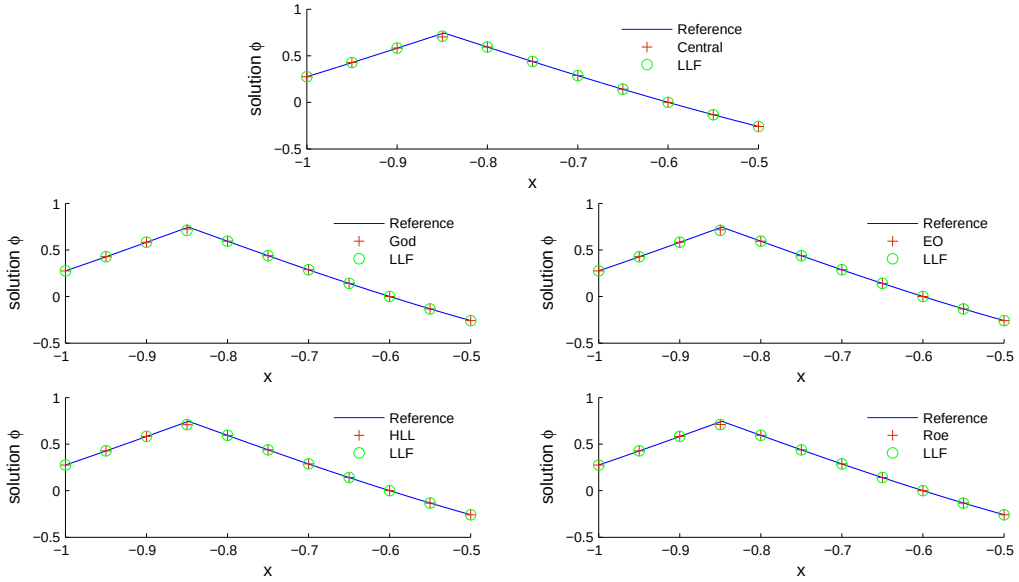

Figure 3: Resolution of discontinuities for example 4.1, **3rd order**, at $T = \frac{1.5}{\pi^2}$, 40 cells, zoomed at the region $-1 \leq x \leq -0.5$ which contains the discontinuous derivative.

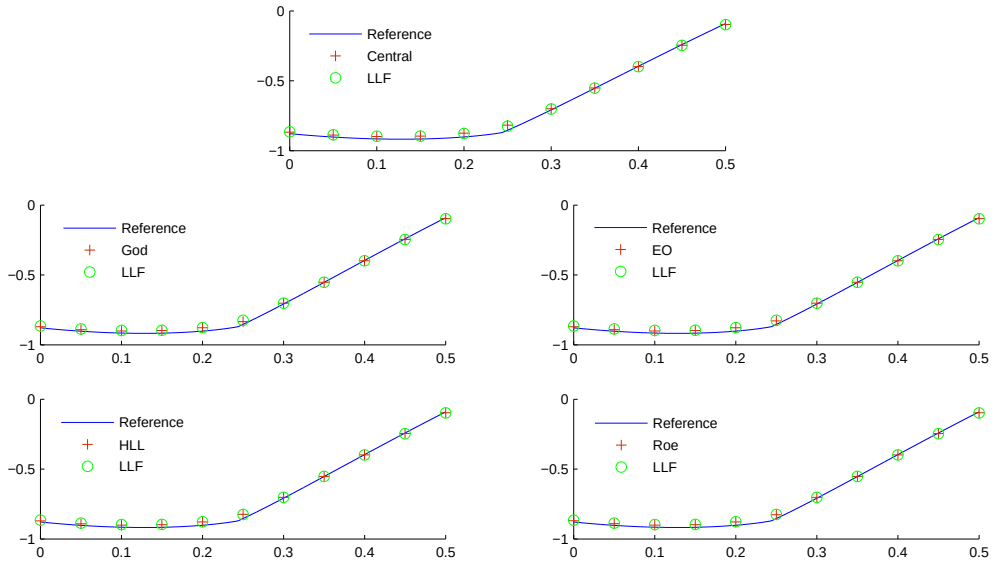

Figure 4: Resolution of discontinuities for 1st order, example 4.2 for $T = \frac{1.5}{\pi^2}$, 40 cells, zoomed at the region $0 \leq x \leq 0.5$ which contains the discontinuous derivative in the solution.

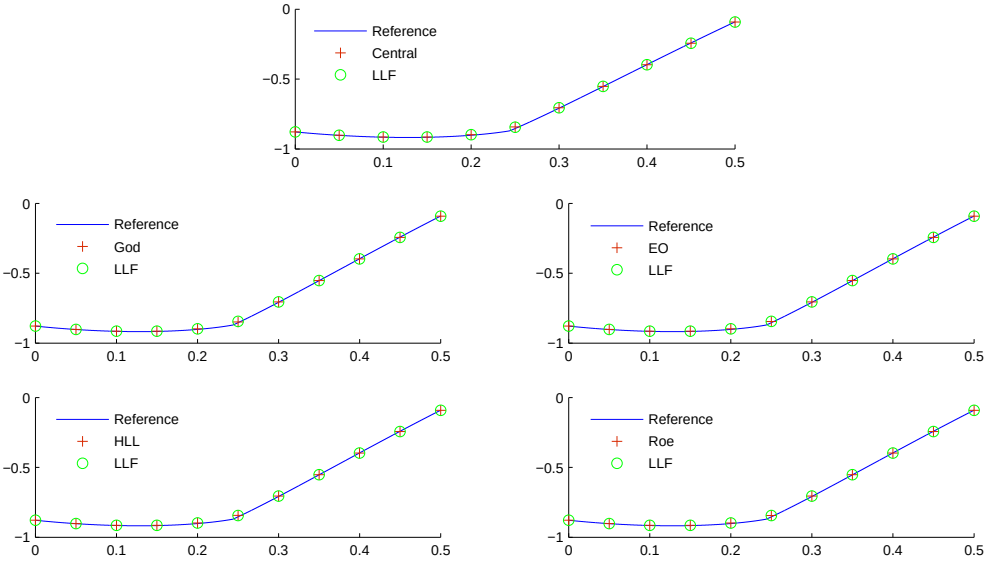

Figure 5: Resolution of discontinuities for 2nd order, example 4.2 for $T = \frac{1.5}{\pi^2}$, 40 cells, zoomed at the region $0 \leq x \leq 0.5$ which contains the discontinuous derivative in the solution.

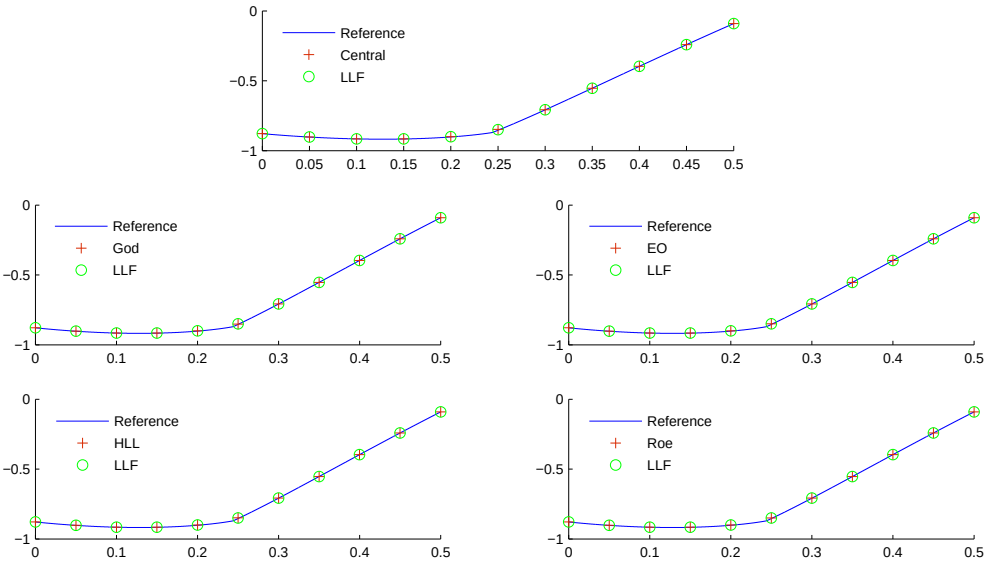

Figure 6: Resolution of discontinuities for 3rd order, example 4.2 for $T = \frac{1.5}{\pi^2}$, 40 cells, zoomed at the region $0 \leq x \leq 0.5$ which contains the discontinuous derivative in the solution.

Table 2: The L_1 and L_∞ errors for example 4.1 using N equally spaced cells with different Hamiltonians at $T = \frac{0.5}{\pi^2}$ for **first** order ENO approximation.

N	Hamiltonian	L_1 error	L_1 order	error ratio	L_∞ error	L_∞ order	error ratio
20	LLF	5.811149E-02		1.000000	5.660415E-02	1.108035	1.000000
	Central	5.870660E-02		1.010240	6.405679E-02	1.211600	1.131662
	God	4.602541E-02		0.792019	4.906337E-02	0.932700	0.866780
	EO	4.665872E-02		0.802917	4.906337E-02	0.932700	0.866780
	HLL	4.797784E-02		0.825617	4.906337E-02	0.932700	0.866780
	Roe	4.807469E-02		0.827284	4.906337E-02	0.932700	0.866780
40	LLF	2.572036E-02	1.218266	1.000000	2.834540E-02	1.033731	1.000000
	Central	2.582158E-02	1.227600	1.003935	3.013726E-02	1.127000	1.063215
	God	2.263060E-02	1.061000	0.879871	2.675172E-02	0.906500	0.943776
	EO	2.272206E-02	1.075400	0.883427	2.675172E-02	0.906500	0.943776
	HLL	2.290488E-02	1.105100	0.890535	2.675172E-02	0.906500	0.943776
	Roe	2.291647E-02	1.107400	0.890986	2.675172E-02	0.906500	0.943776
80	LLF	1.195806E-02	1.124800	1.000000	1.456808E-02	0.977600	1.000000
	Central	1.197293E-02	1.128800	1.001244	1.507655E-02	1.017200	1.034903
	God	1.118225E-02	1.035400	0.935123	1.405883E-02	0.944900	0.965043
	EO	1.119229E-02	1.040000	0.935963	1.405883E-02	0.944900	0.965043
	HLL	1.121537E-02	1.048700	0.937892	1.405883E-02	0.944900	0.965043
	Roe	1.122036E-02	1.048800	0.938310	1.405883E-02	0.944900	0.965043
160	LLF	5.744098E-03	1.067400	1.000000	7.353236E-03	0.995300	1.000000
	Central	5.746095E-03	1.068700	1.000348	7.474004E-03	1.021500	1.016424
	God	5.550256E-03	1.019700	0.966254	7.232450E-03	0.967600	0.983574
	EO	5.550870E-03	1.020800	0.966361	7.232450E-03	0.967600	0.983574
	HLL	5.553232E-03	1.023200	0.966772	7.232450E-03	0.967600	0.983574
	Roe	5.555112E-03	1.023400	0.967099	7.232450E-03	0.967600	0.983574
320	LLF	2.813035E-03	1.034600	1.000000	3.692982E-03	0.998100	1.000000
	Central	2.813290E-03	1.035000	1.000091	3.723830E-03	1.009600	1.008353
	God	2.764664E-03	1.010000	0.982805	3.662134E-03	0.986200	0.991647
	EO	2.764664E-03	1.010100	0.982805	3.662134E-03	0.986200	0.991647
	HLL	2.764671E-03	1.010800	0.982807	3.662134E-03	0.986200	0.991647
	Roe	2.765300E-03	1.010900	0.983031	3.662134E-03	0.986200	0.991647

For L^1 error, when $20 \le N \le 320$:

$$\text{ENO-Central} \gg \text{ENO-LLF} \gg \text{ENO-Roe} \gg \text{ENO-HLL} \gg \text{ENO-EO} \gg \text{ENO-God}.$$

For L^∞ error, when $20 \le N \le 320$:

$$\text{ENO-Central} \gg \text{ENO-LLF} \gg \text{ENO-Roe} \approx \text{ENO-HLL} \approx \text{ENO-EO} \approx \text{ENO-God}.$$

We analyze the resolution of discontinuities for different Hamiltonians at time $T = \frac{1.5}{\pi^2}$ when the solution has a discontinuous derivative. In Figures 1-3, we show the resolution of discontinuities when the number of cells is 40 for the 1st, 2nd and 3rd order schemes respectively, for the different Hamiltonians in comparison with the reference "exact" solution, and against the ENO-LLF scheme on the same mesh, zoomed at the region $-1 \le x \le -0.5$ which contains the discontinuous derivative in the solution. Solid lines

Table 3: The L_1 and L_∞ errors for example 4.1 using N equally spaced cells with different Hamiltonians at $T = \frac{0.5}{\pi^2}$ for **second** order ENO approximation.

N	Hamiltonian	L_1 error	L_1 order	error ratio	L_∞ error	L_∞ order	error ratio
20	LLF	1.290435E-02		1.000000	2.322905E-02	1.518241	1.000000
	Central	1.302880E-02		1.009644	2.346184E-02	1.629285	1.010022
	God	1.252567E-02		0.970655	2.296735E-02	1.379072	0.988734
	EO	1.255913E-02		0.973248	2.296735E-02	1.379072	0.988734
	HLL	1.260554E-02		0.976844	2.296735E-02	1.379072	0.988734
	Roe	1.257924E-02		0.974807	2.296735E-02	1.379072	0.988734
40	LLF	3.247373E-03	2.062206	1.000000	6.871831E-03	1.820452	1.000000
	Central	3.253705E-03	2.073640	1.001950	6.888440E-03	1.831748	1.002417
	God	3.224817E-03	2.028107	0.993054	6.853551E-03	1.807500	0.997340
	EO	3.225019E-03	2.032000	0.993116	6.853551E-03	1.807500	0.997340
	HLL	3.225516E-03	2.037282	0.993269	6.853551E-03	1.807500	0.997340
	Roe	3.225500E-03	2.034169	0.993264	6.853551E-03	1.807500	0.997340
80	LLF	8.234437E-04	2.015204	1.000000	1.791772E-03	1.974256	1.000000
	Central	8.238159E-04	2.017402	1.000452	1.792958E-03	1.976830	1.000662
	God	8.220807E-04	2.007400	0.998345	1.790587E-03	1.971316	0.999339
	EO	8.220807E-04	2.007492	0.998345	1.790587E-03	1.971316	0.999339
	HLL	8.220807E-04	2.007719	0.998345	1.790587E-03	1.971316	0.999339
	Roe	8.220807E-04	2.007712	0.998345	1.790587E-03	1.971316	0.999339
160	LLF	2.073057E-04	2.007846	1.000000	4.478901E-04	2.018199	1.000000
	Central	2.073288E-04	2.008342	1.000111	4.479530E-04	2.018958	1.000141
	God	2.072225E-04	2.006019	0.999599	4.478247E-04	2.017449	0.999854
	EO	2.072225E-04	2.006019	0.999599	4.478247E-04	2.017449	0.999854
	HLL	2.072225E-04	2.006019	0.999599	4.478247E-04	2.017449	0.999854
	Roe	2.072225E-04	2.006019	0.999599	4.478247E-04	2.017449	0.999854
320	LLF	5.206606E-05	2.002330	1.000000	1.104883E-04	2.028353	1.000000
	Central	5.206751E-05	2.002451	1.000028	1.104915E-04	2.028515	1.000029
	God	5.206095E-05	2.001891	0.999902	1.104845E-04	2.028192	0.999965
	EO	5.206095E-05	2.001891	0.999902	1.104845E-04	2.028192	0.999965
	HLL	5.206095E-05	2.001891	0.999902	1.104845E-04	2.028192	0.999965
	Roe	5.206095E-05	2.001891	0.999902	1.104845E-04	2.028192	0.999965

For L^1 error, for $20 \leq N \leq 40$:

$$\text{ENO-Central} \gg \text{ENO-LLF} \gg \text{ENO-HLL} \gg \text{ENO-Roe} \gg \text{ENO-EO} \gg \text{ENO-God},$$

For L^1 error, for $80 \leq N \leq 320$:

$$\text{ENO-Central} \gg \text{ENO-LLF} \gg \text{ENO-HLL} \approx \text{ENO-Roe} \approx \text{ENO-EO} \approx \text{ENO-God}.$$

For L^∞ error, for $20 \leq N \leq 320$:

$$\text{ENO-Central} \gg \text{ENO-LLF} \gg \text{ENO-HLL} \approx \text{ENO-Roe} \approx \text{ENO-EO} \approx \text{ENO-God}.$$

indicate the reference "exact" solution, hollow circles indicate scheme with ENO-LLF, and the plus symbols represent the scheme with respective schemes given in the graphs.

For small number of cells N, and first, second and third order of accuracy, the resolution of the ENO-Central scheme is the worst among all the schemes. The resolution of the

Table 4: The L_1 and L_∞ errors for example 4.1 using N equally spaced cells with different Hamiltonians at $T = \frac{0.5}{\pi^2}$ for **third** order ENO approximation.

N	Hamiltonian	L_1 error	L_1 order	error ratio	L_∞ error	L_∞ order	error ratio
20	LLF	1.998844E-03		1.000000	3.855039E-03	2.211814	1.000000
	Central	2.008514E-03		1.004838	3.865339E-03	2.292774	1.002672
	God	1.986424E-03		0.993786	3.844542E-03	2.122905	0.997277
	EO	1.986447E-03		0.993798	3.844542E-03	2.122905	0.997277
	HLL	1.986756E-03		0.993953	3.844542E-03	2.122905	0.997277
	Roe	1.988028E-03		0.994589	3.844542E-03	2.122905	0.997277
40	LLF	2.610490E-04	3.042549	1.000000	5.860125E-04	2.815629	1.000000
	Central	2.611923E-04	3.048941	1.000549	5.861887E-04	2.819168	1.000301
	God	2.608595E-04	3.034318	0.999274	5.858379E-04	2.811999	0.999702
	EO	2.608595E-04	3.034335	0.999274	5.858379E-04	2.811999	0.999702
	HLL	2.608595E-04	3.034568	0.999274	5.858379E-04	2.811999	0.999702
	Roe	2.608595E-04	3.035525	0.999274	5.858379E-04	2.811999	0.999702
80	LLF	3.282535E-05	3.045347	1.000000	7.650053E-05	2.990325	1.000000
	Central	3.282749E-05	3.046057	1.000065	7.650332E-05	2.990712	1.000036
	God	3.282247E-05	3.044409	0.999912	7.649783E-05	2.989939	0.999965
	EO	3.282247E-05	3.044409	0.999912	7.649783E-05	2.989939	0.999965
	HLL	3.282247E-05	3.044409	0.999912	7.649783E-05	2.989939	0.999965
	Roe	3.282247E-05	3.044409	0.999912	7.649783E-05	2.989939	0.999965
160	LLF	4.067356E-06	3.039802	1.000000	1.011282E-05	2.945598	1.000000
	Central	4.067388E-06	3.039886	1.000008	1.011285E-05	2.945646	1.000003
	God	4.067312E-06	3.039690	0.999989	1.011278E-05	2.945552	0.999997
	EO	4.067312E-06	3.039690	0.999989	1.011278E-05	2.945552	0.999997
	HLL	4.067312E-06	3.039690	0.999989	1.011278E-05	2.945552	0.999997
	Roe	4.067312E-06	3.039690	0.999989	1.011278E-05	2.945552	0.999997
320	LLF	5.085965E-07	3.013018	1.000000	1.315564E-06	2.955695	1.000000
	Central	5.085970E-07	3.013028	1.000001	1.315564E-06	2.955699	1.000000
	God	5.085959E-07	3.013004	0.999999	1.315563E-06	2.955691	1.000000
	EO	5.085959E-07	3.013004	0.999999	1.315563E-06	2.955691	1.000000
	HLL	5.085959E-07	3.013004	0.999999	1.315563E-06	2.955691	1.000000
	Roe	5.085959E-07	3.013004	0.999999	1.315563E-06	2.955691	1.000000

For L^1 error, for $N = 20$:

$$\text{ENO-Central} \gg \text{ENO-LLF} \gg \text{ENO-Roe} \gg \text{ENO-HLL} \gg \text{ENO-EO} \gg \text{ENO-God}.$$

For L^1 error, for $40 \leq N \leq 320$:

$$\text{ENO-Central} \gg \text{ENO-LLF} \gg \text{ENO-Roe} \approx \text{ENO-HLL} \approx \text{ENO-EO} \approx \text{ENO-God}.$$

For L^∞ error, for $20 \leq N \leq 320$:

$$\text{ENO-Central} \gg \text{ENO-LLF} \gg \text{ENO-Roe} \approx \text{ENO-HLL} \approx \text{ENO-EO} \approx \text{ENO-God}.$$

ENO-God and ENO-EO scheme are the best, followed by the ENO-Roe scheme, followed closely by that of the ENO-LLF scheme, followed by the ENO-HLL scheme. As the number of cells is increased, for orders of accuracy 1,2 and 3, the resolution of the ENO-Central scheme continues to remain the worst among all the schemes and that of the

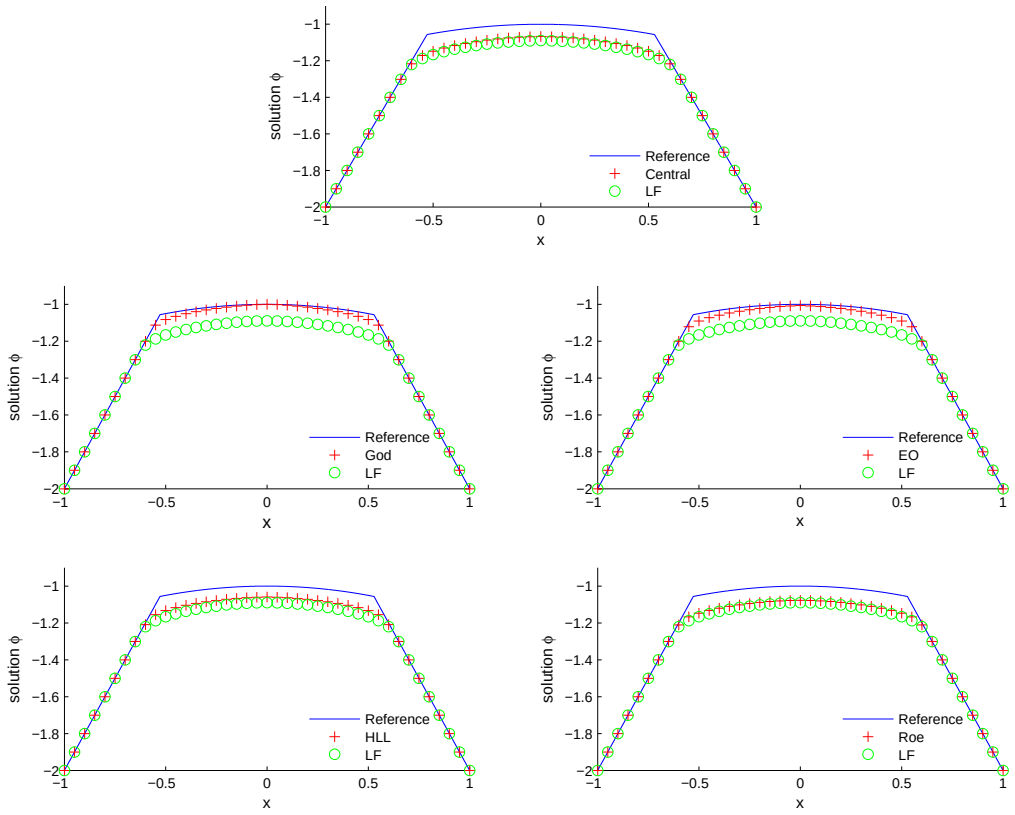

Figure 7: Resolution of discontinuities for 1st order, example 4.3 for $T = 1$, 40 cells, on the whole domain $-1 \leq x \leq 1$.

ENO-God and ENO-EO scheme the best. However, there is a change in the performance of the other schemes. ENO-God and ENO-EO schemes are followed by the ENO-HLL scheme which is followed by ENO-Roe scheme which is followed by ENO-LF scheme for the resolution of discontinuities.

Example 4.2. We repeat the numerical experiments of the previous example for another standard test case from [24], a 1-dimensional HJ equation given by

$$\begin{aligned} \phi_t - \cos(\phi + 1) &= 0, \qquad -1 \leq x \leq 1, \\ \phi(x, 0) &= -\cos \pi x. \end{aligned}$$

The Hamiltonian is non-convex. Here again, as in the previous example we use periodic boundary conditions and compute the solution and test accuracy when it is smooth, that is, at $t = \frac{0.5}{\pi^2}$.

All the schemes give the desired accuracy in space. The numerical results for accuracy and resolution of discontinuities are very similar to that of the convex Hamiltonian (Example 4.1) case, however for the first order case, the efficiency of using particular

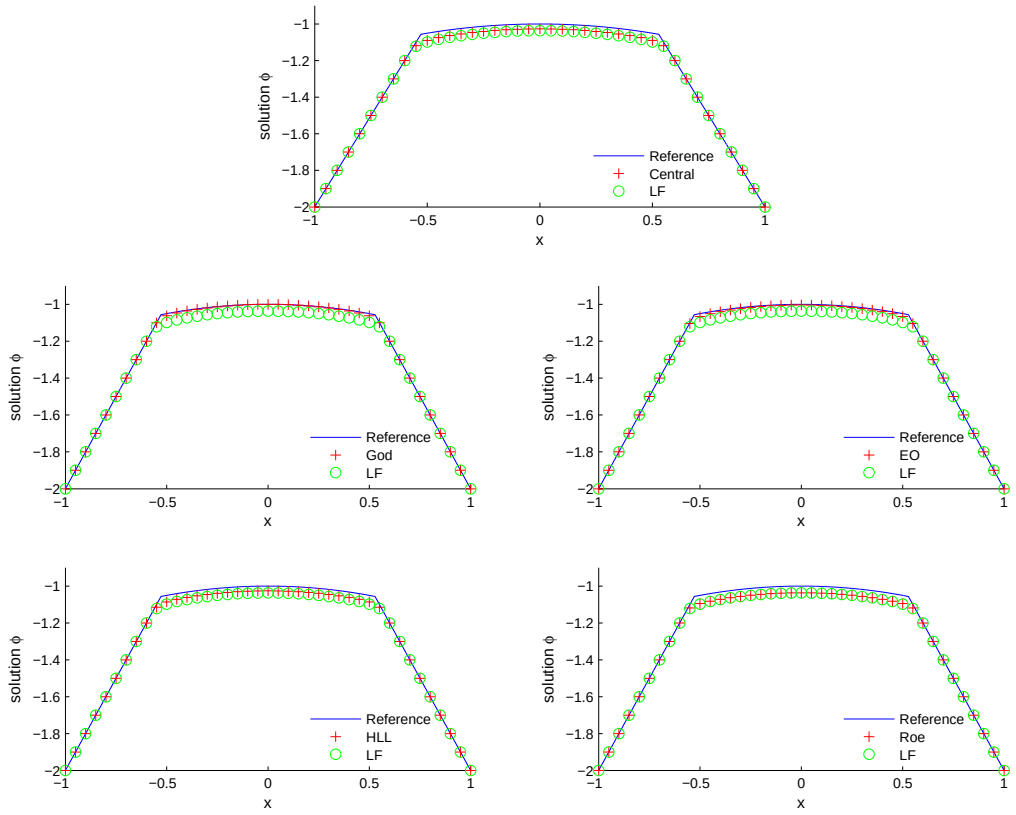

Figure 8: Resolution of discontinuities for 2nd order, example 4.3 for $T = 1$, 40 cells, on the whole domain $-1 \leq x \leq 1$.

Hamiltonian is more pronounced than in the case of Example 4.1. For first order scheme, ENO-Central gives the largest and ENO-God gives the smallest L_1 and L^∞ errors among all the schemes. For small number of cells ($N = 20, 40$), the L^1 error by ENO-God, ENO-EO are about $70 - 80\%$ of the L^1 error by ENO-LLF and the L^1 error by ENO-HLL and ENO-Roe are about $80 - 85\%$ of the L^1 error by ENO-LLF. As the number of cells increase ($N \geq 80$), the error by ENO-God, ENO-EO, ENO-HLL and ENO-Roe are about $90 - 97\%$ of the L^1 error by ENO-LLF. For the second and third order schemes, we can see from Tables 3 and 4 that for small number of cells ENO-Central gives the largest and ENO-God gives the smallest L_1 error, but as the number of cells is increased, the errors become very close to each other as in the convex Hamiltonian case.

We analyze the resolution of discontinuities for different Hamiltonians at time $T = \frac{1.5}{\pi^2}$ when the solution has two discontinuous derivatives. In Figures 4-6, we show the resolution of discontinuities when the number of cells is 40 for the first, second and third order schemes respectively, for the different Hamiltonians in comparison with the reference "exact" solution, and against the ENO-LLF scheme on the same mesh, zoomed at the

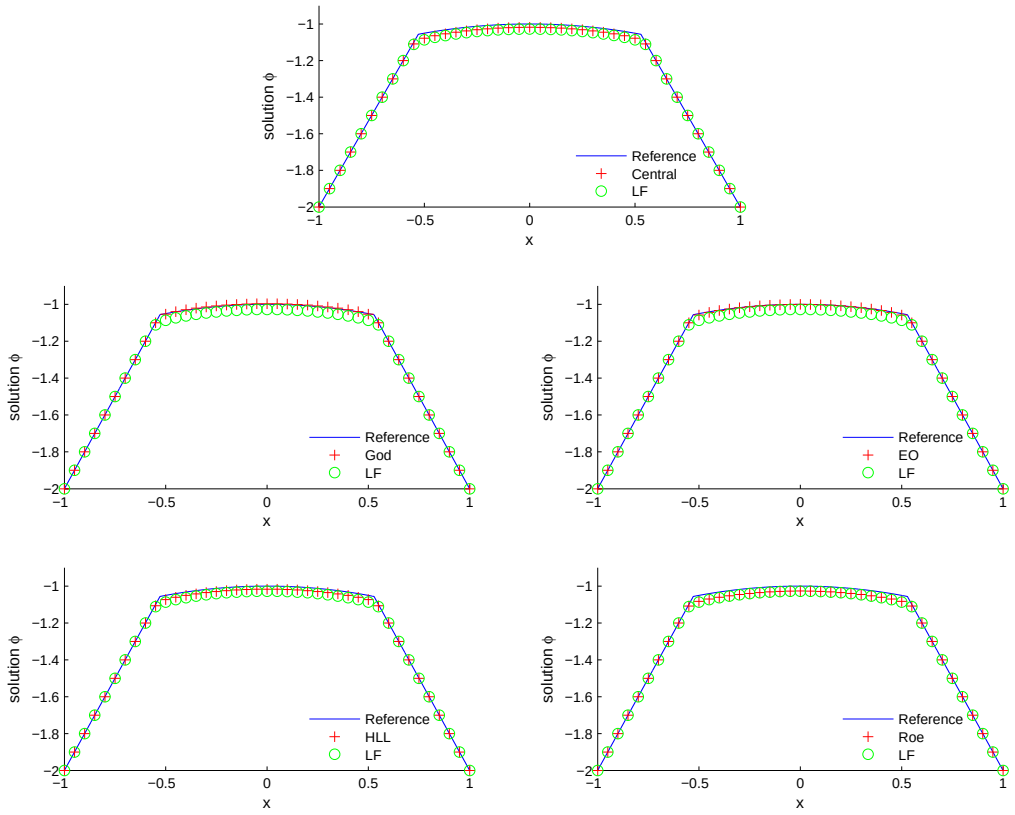

Figure 9: Resolution of discontinuities for 3rd order, example 4.3 for $T = 1$, 40 cells, on the whole domain $-1 \leq x \leq 1$.

region $0 \leq x \leq 0.5$ which contains one of the discontinuous derivatives. In regard to resolution of discontinuities all the Hamiltonians behave exactly the same as the case of Example 4.1.

Example 4.3. We work with an example in [18], a 1-dimensional Riemann problem with non-convex Hamiltonian given by

$$\begin{aligned} \phi_t + \frac{1}{4}(\phi_x^2 - 1)(\phi_x^2 - 4) &= 0, \qquad -1 \leq x \leq 1, \\ \phi(x, 0) &= -2|x|. \end{aligned}$$

Since the initial condition is linear, we use linear extrapolation for the boundary points.

We analyze the resolution of discontinuities for different Hamiltonians at time $T = 1$ when the solution has discontinuous derivatives. In Figures 7, 8 and 9 we show the resolution of discontinuities when the number of cells is 40 for the first, second and third order schemes respectively, for the different Hamiltonians in comparison with the reference

"exact" solution, and against the ENO-LLF scheme on the same mesh, over the domain $-1 \leq x \leq 1$ which contains the discontinuous derivatives in the solution.

From the figures, we can see that the approximate solution becomes closer to the reference solution when the number of cells is increased and the order of the approximation is increased. In the previous two examples, ENO-Central was the worst in the resolution of discontinuities. However for the Riemann problem, ENO-LLF scheme serves to be the worst for orders of accuracy 1, 2 and 3. The resolution of the ENO-God and ENO-EO scheme are the best, followed by the ENO-HLL scheme. There is a change in the performance of the ENO-Roe and ENO-Central as the order is increased and as the number of cells is increased. For 1st order and small number of cells, the ENO-Roe scheme is superior to the ENO-Central scheme. However as the order is increased along with the number of cells, the ENO-Central scheme takes over and seems to be slightly better than the ENO-Roe at resolving discontinuities.

We perform tests on one two-dimensional example. Study is performed addressing issues of CPU cost and numerical accuracy. The reference "exact" solution is computed using a fifth order WENO [16, 26] and fourth order TVD Runge-Kutta [9, 8] using 1280×1280 cells. The CFL number is taken to be 0.1 for the first, second and third order accuracy.

Example 4.4. We work with an example in [24], a 2-dimensional HJ equation given by

$$\begin{aligned} \phi_t + \frac{(\phi_x + \phi_y + 1)^2}{2} &= 0, \qquad -2 \leq x, y \leq 2, \\ \phi(x, y, 0) &= -\cos \pi(\frac{x+y}{2}). \end{aligned}$$

For the two-dimensional example we make comparison only between four Hamiltonians ENO-LLF, ENO-Central, ENO-HLL and ENO-Roe. We use periodic boundary conditions and compute the solution and test accuracy when it is smooth, that is, up to time $T = \frac{0.1}{\pi^2}$. The reference "exact" solution is computed using a fifth order WENO [16, 26] and fourth order TVD Runge-Kutta [8, 9] using 1280×1280 cells as in the one-dimensional case. In Table 5, we provide a CPU time comparison for the ENO scheme with different Hamiltonians. The numerical errors and the orders of accuracy for the numerical solution ϕ_j^n, and ratios of the numerical errors for cells up to 320×320 in comparison with the LLF scheme are shown in Tables 6-8.

The sum of the CPU times for $N = 10 \times 10, 20 \times 20, 40 \times 40, 80 \times 80, 160 \times 160$ and 320×320 cells is recorded in Table 5. The ENO-LLF takes the least amount of time followed closely by the ENO-Central scheme. ENO-Roe takes about 2 times the time taken by the

Table 5: Total CPU time in seconds for the RKFD method with ENO approximation with different Hamiltonians. The sum of the CPU times for $N = 10, 20, 40, 80, 160, 320, 640$ and 1280 cells is recorded for Example 4.4 for orders 1, 2, and 3.

Order	LLF	Central	HLL	Roe
1	154.69	161.97	867.16	284.91
2	308.98	323.61	1733.91	569.42
3	617.00	646.23	3466.33	1137.67

Table 6: The L_1 and L_∞ errors for example 4.1 using N equally spaced cells with different Hamiltonians at $T = \frac{0.1}{\pi^2}$ for **first** order ENO approximation.

N × N	Hamiltonian	L_1 error	L_1 order	error ratio	L_∞ error	L_∞ order	error ratio
10 × 10	LLF	3.424963E-01		1.000000	2.763178E-02		1.000000
	Central	2.687962E-01		0.784815	2.612001E-02		0.945289
	HLL	1.796082E-01		0.524409	1.856118E-02		0.671733
	Roe	2.014738E-01		0.588251	1.856118E-02		0.671733
20 × 20	LLF	1.087766E-01	1.773765	1.000000	1.077102E-02	1.456957	1.000000
	Central	9.433678E-02	1.619298	0.867252	1.037421E-02	1.427992	0.963160
	HLL	7.636378E-02	1.322662	0.702024	8.389839E-03	1.227989	0.778927
	Roe	7.673543E-02	1.492816	0.705440	8.389839E-03	1.227989	0.778927
40 × 40	LLF	4.040246E-02	1.480317	1.000000	4.742109E-03	1.226182	1.000000
	Central	4.040095E-02	1.267496	0.999963	4.675746E-03	1.191144	0.986005
	HLL	3.565142E-02	1.138510	0.882407	4.313883E-03	0.994220	0.909697
	Roe	3.571398E-02	1.143146	0.883955	4.313883E-03	0.994220	0.909697
80 × 80	LLF	1.855344E-02	1.142989	1.000000	2.246983E-03	1.096958	1.000000
	Central	1.855331E-02	1.142945	0.999993	2.277247E-03	1.056610	1.013469
	HLL	1.733488E-02	1.059028	0.934322	2.186449E-03	0.998065	0.973060
	Roe	1.734896E-02	1.060411	0.935080	2.186449E-03	0.998065	0.973060
160 × 160	LLF	8.847578E-03	1.077962	1.000000	1.113432E-03	1.022106	1.000000
	Central	8.847571E-03	1.077953	0.999999	1.121015E-03	1.031702	1.006810
	HLL	8.539154E-03	1.030721	0.965140	1.098266E-03	1.002316	0.986379
	Roe	8.542604E-03	1.031314	0.965530	1.098266E-03	1.002316	0.986379
320 × 320	LLF	4.298191E-03	1.046248	1.000000	5.515409E-04	1.018042	1.000000
	Central	4.298191E-03	1.046247	1.000000	5.534388E-04	1.022900	1.003441
	HLL	4.220630E-03	1.021217	0.981955	5.477450E-04	1.008176	0.993118
	Roe	4.221512E-03	1.021500	0.982160	5.477450E-04	1.008176	0.993118

For L^1 error, for $10 \leq N \leq 320$:

$$\text{ENO-LLF} \gg \text{ENO-Central} \gg \text{ENO-Roe} \gg \text{ENO-HLL}.$$

For L^∞ error, for $10 \leq N \leq 40$:

$$\text{ENO-LLF} \gg \text{ENO-Central} \gg \text{ENO-Roe} \approx \text{ENO-HLL}.$$

For L^∞ error, for $80 \leq N \leq 320$:

$$\text{ENO-Central} \gg \text{ENO-LLF} \gg \text{ENO-Roe} \approx \text{ENO-HLL}.$$

ENO-LLF for all orders and the ENO-HLL takes about $5-6$ times the time taken by the ENO-LLF for all orders.

Unlike Examples 4.1 and 4.2 of 1-dimensional case, for first order scheme, ENO-LLF gives the largest and ENO-HLL gives the smallest L_1 error among all the Hamiltonians. For small number of cells ($N = 10 \times 10, 20 \times 20$), the L^1 error by ENO-Central is about $78-87\%$ of the L^1 error by ENO-LLF and as the number of cells increase ($N \geq 40 \times 40$), ENO-Central and ENO-LLF errors every close to each other. Also for small number of cells ($N = 10 \times 10, 20 \times 20$), the L^1 error by ENO-HLL and ENO-Roe are about $50-70\%$

Table 7: The L_1 and L_∞ errors for example 4.1 using N equally spaced cells with different Hamiltonians at $T = \frac{0.1}{\pi^2}$ for **second** order ENO approximation.

N × N	Hamiltonian	L_1 error	L_1 order	error ratio	L_∞ error	L_∞ order	error ratio
10 × 10	LLF	9.335852E-02		1.000000	1.486144E-02		1.000000
	Central	9.356142E-02		1.002173	1.508833E-02		1.015267
	HLL	8.423839E-02		0.902311	1.439668E-02		0.968727
	Roe	8.423839E-02		0.902311	1.439668E-02		0.968727
20 × 20	LLF	2.293862E-02	2.170687	1.000000	4.757439E-03	1.761541	1.000000
	Central	2.295080E-02	2.173224	1.000531	4.776947E-03	1.778644	1.004101
	HLL	2.241890E-02	2.047156	0.977343	4.718081E-03	1.725253	0.991727
	Roe	2.242336E-02	2.046848	0.977537	4.718081E-03	1.725253	0.991727
40 × 40	LLF	5.198243E-03	2.218821	1.000000	1.206735E-03	2.050357	1.000000
	Central	5.198882E-03	2.219430	1.000123	1.207830E-03	2.055119	1.000907
	HLL	5.166391E-03	2.193753	0.993872	1.204471E-03	2.040748	0.998124
	Roe	5.166391E-03	2.194051	0.993872	1.204471E-03	2.040748	0.998124
80 × 80	LLF	1.268981E-03	2.071014	1.000000	3.218475E-04	1.941020	1.000000
	Central	1.269011E-03	2.071160	1.000024	3.219161E-04	1.942038	1.000213
	HLL	1.267048E-03	2.064226	0.998477	3.216948E-04	1.938959	0.999526
	Roe	1.267048E-03	2.064226	0.998477	3.216948E-04	1.938959	0.999526
160 × 160	LLF	3.150373E-04	2.028194	1.000000	8.184242E-05	1.993263	1.000000
	Central	3.150393E-04	2.028219	1.000006	8.184648E-05	1.993501	1.000050
	HLL	3.149181E-04	2.026526	0.999622	8.183257E-05	1.992747	0.999880
	Roe	3.149181E-04	2.026526	0.999622	8.183257E-05	1.992747	0.999880
320 × 320	LLF	7.855222E-05	2.012831	1.000000	2.088876E-05	1.979002	1.000000
	Central	7.855235E-05	2.012838	1.000002	2.088902E-05	1.979056	1.000012
	HLL	7.854484E-05	2.012419	0.999906	2.088813E-05	1.978872	0.999969
	Roe	7.854484E-05	2.012419	0.999906	2.088813E-05	1.978872	0.999969

For L^1 error, for $N = 10$:

$$\text{ENO-LLF} \gg \text{ENO-Central} \gg \text{ENO-Roe} \gg \text{ENO-HLL}.$$

For L^1 error, for $20 \leq N \leq 40$:

$$\text{ENO-Central} \gg \text{ENO-LLF} \gg \text{ENO-Roe} \gg \text{ENO-HLL}.$$

For L^1 error, for $80 \leq N \leq 320$:

$$\text{ENO-Central} \gg \text{ENO-LLF} \gg \text{ENO-Roe} \approx \text{ENO-HLL}.$$

For L^∞ error, for $10 \leq N \leq 320$:

$$\text{ENO-Central} \gg \text{ENO-LLF} \gg \text{ENO-Roe} \approx \text{ENO-HLL}.$$

of the L^1 error by ENO-LLF and as the number of cells increase ($N \geq 40 \times 40$), error by ENO-HLL and ENO-Roe are about $90 - 98\%$ of the L^1 error by ENO-LLF.

For the second and third order schemes, we can see from Tables 7 and 8 that for small number of cells ENO-Central gives the largest and ENO-HLL gives the smallest L_1 error among all the Hamiltonians but as the number of cells is increased, the errors become very close to each other.

Table 8: The L_1 and L_∞ errors for example 4.1 using N equally spaced cells with different Hamiltonians at $T = \frac{0.1}{\pi^2}$ for **third** order ENO approximation.

N × N	Hamiltonian	L_1 error	L_1 order	error ratio	L_∞ error	L_∞ order	error ratio
10 × 10	LLF	1.565009E-02	1.000000		1.620281E-03		1.000000
	Central	1.564968E-02	0.999974		1.617109E-03		0.998042
	HLL	1.523907E-02	0.973737		1.600033E-03		0.987503
	Roe	1.523907E-02	0.973737		1.600033E-03		0.987503
20 × 20	LLF	1.883497E-03	3.274447	1.000000	2.022829E-04	3.217756	1.000000
	Central	1.883723E-03	3.274221	1.000120	2.022137E-04	3.215254	0.999658
	HLL	1.877804E-03	3.237970	0.996977	2.018678E-04	3.201485	0.997948
	Roe	1.877804E-03	3.237970	0.996977	2.018678E-04	3.201485	0.997948
40 × 40	LLF	2.124377E-04	3.261697	1.000000	2.464951E-05	3.146119	1.000000
	Central	2.124410E-04	3.261853	1.000016	2.464863E-05	3.145661	0.999964
	HLL	2.123519E-04	3.257775	0.999596	2.464422E-05	3.143370	0.999785
	Roe	2.123519E-04	3.257775	0.999596	2.464422E-05	3.143370	0.999785
80 × 80	LLF	2.538874E-05	3.120009	1.000000	3.189839E-06	3.003166	1.000000
	Central	2.538879E-05	3.120030	1.000002	3.189876E-06	3.003096	1.000012
	HLL	2.538743E-05	3.119492	0.999948	3.189763E-06	3.002885	0.999976
	Roe	2.538743E-05	3.119492	0.999948	3.189763E-06	3.002885	0.999976
160 × 160	LLF	3.111871E-06	3.055631	1.000000	4.074357E-07	2.995599	1.000000
	Central	3.111872E-06	3.055633	1.000000	4.074363E-07	2.995614	1.000001
	HLL	3.111851E-06	3.055565	0.999993	4.074346E-07	2.995569	0.999997
	Roe	3.111851E-06	3.055565	0.999993	4.074346E-07	2.995569	0.999997
320 × 320	LLF	3.856748E-07	3.025904	1.000000	5.143520E-08	2.999203	1.000000
	Central	3.856748E-07	3.025904	1.000000	5.143521E-08	2.999205	1.000000
	HLL	3.856744E-07	3.025896	0.999999	5.143518E-08	2.999200	1.000000
	Roe	3.856744E-07	3.025896	0.999999	5.143518E-08	2.999200	1.000000

For L^1 error, for $N = 10$:

$$\text{ENO-LLF} \gg \text{ENO-Central} \gg \text{ENO-Roe} \approx \text{ENO-HLL}.$$

For L^1 error, for $20 \leq N \leq 160$:

$$\text{ENO-Central} \gg \text{ENO-LLF} \gg \text{ENO-Roe} \gg \text{ENO-HLL}.$$

For L^1 error, for $N = 320$:

$$\text{ENO-Central} \approx \text{ENO-LLF} \gg \text{ENO-Roe} \approx \text{ENO-HLL}.$$

For L^∞ error, for $10 \leq N \leq 40$:

$$\text{ENO-LLF} \gg \text{ENO-Central} \gg \text{ENO-Roe} \approx \text{ENO-HLL}.$$

For L^∞ error, for $80 \leq N \leq 320$:

$$\text{ENO-Central} \gg \text{ENO-LLF} \gg \text{ENO-Roe} \approx \text{ENO-HLL}.$$

5. Conclusion

In this paper, we have studied and compared six different numerical Hamiltonians for the RKFD methods. Extensive 1-dimensional numerical tests performed on Hamilton-Jacobi equations indicate Hamiltonians with upwinding property perform the best when

factors such as numerical accuracy and resolution of kinks in the solution are addressed. The RKFD method with ENO approximation with LLF and Central Hamiltonian cost the least CPU time among all, but the numerical errors and resolution of discontinuities are also the worst among all. The RKFD methods with Godunov Hamiltonian seem to cost significantly more CPU time than the RKFD-LLF method. The HLL, Roe, EO Hamiltonians might be good choices as Hamiltonians when all factors such as the cost of CPU time, numerical accuracy and resolution of discontinuities in the solution are considered. However we should keep in mind that as we increase the order of accuracy of the ENO approximation and increase the number of cells, the errors for all Hamiltonians are nearly equal.

Acknowledgments

This research was supported by the National Science Foundation under Grant DMS05-05975.

References

[1] S. Bryson, A. Kurganov, D. Levy, and G. Petrova. Semi-discrete central-upwind schemes with reduced dissipation for Hamilton-Jacobi equations. *IMA J. Numer. Anal.*, 25(1):113–138, 2005.

[2] S. Bryson and D. Levy. High-order semi-discrete central-upwind schemes for multi-dimensional Hamilton-Jacobi equations. *J. Comput. Phys.*, 189(1):63–87, 2003.

[3] M. G. Crandall and P.-L. Lions. Viscosity solutions of Hamilton-Jacobi equations. *Trans. Amer. Math. Soc.*, 277(1):1–42, 1983.

[4] M. G. Crandall and P.-L. Lions. Two approximations of solutions of Hamilton-Jacobi equations. *Math. Comp.*, 43(167):1–19, 1984.

[5] B. Engquist and S. Osher. One-sided difference approximations for nonlinear conservation laws. *Math. Comp.*, 36(154):321–351, 1981.

[6] B. Engquist and O. Runborg. Computational high frequency wave propagation. *Acta Numer.*, 12:181–266, 2003.

[7] L. C. Evans. *Partial differential equations*, volume 19 of *Graduate Studies in Mathematics*. American Mathematical Society, Providence, RI, 1998.

[8] S. Gottlieb and C.-W. Shu. Total variation diminishing Runge-Kutta schemes. *Math. Comp.*, 67(221):73–85, 1998.

[9] S. Gottlieb, C.-W. Shu, and E. Tadmor. Strong stability-preserving high-order time discretization methods. *SIAM Rev.*, 43(1):89–112 (electronic), 2001.

[10] A. Harten. Preliminary results on the extension of ENO schemes to two-dimensional problems. In *Nonlinear hyperbolic problems (St. Etienne, 1986)*, volume 1270 of *Lecture Notes in Math.*, pages 23–40. Springer, Berlin, 1987.

[11] A. Harten, S. Engquist, Björn and, and S. R. Chakravarthy. Uniformly high-order accurate essentially nonoscillatory schemes. III. *J. Comput. Phys.*, 71(2):231–303, 1987.

[12] A. Harten, P. D. Lax, and B. van Leer. On upstream differencing and Godunov-type schemes for hyperbolic conservation laws. *SIAM Rev.*, 25(1):35–61, 1983.

[13] A. Harten and S. Osher. Uniformly high-order accurate nonoscillatory schemes. I. *SIAM J. Numer. Anal.*, 24(2):279–309, 1987.

[14] C. Hu and C.-W. Shu. A discontinuous Galerkin finite element method for Hamilton-Jacobi equations. *SIAM J. Sci. Comput.*, 21(2):666–690 (electronic), 1999.

[15] G.-S. Jiang and D. Peng. Weighted ENO schemes for Hamilton-Jacobi equations. *SIAM J. Sci. Comput.*, 21(6):2126–2143 (electronic), 2000.

[16] G.-S. Jiang and C.-W. Shu. Efficient implementation of weighted ENO schemes. *J. Comput. Phys.*, 126(1):202–228, 1996.
[17] A. Kurganov, S. Noelle, and G. Petrova. Semidiscrete central-upwind schemes for hyperbolic conservation laws and Hamilton-Jacobi equations. *SIAM J. Sci. Comput.*, 23(3):707–740 (electronic), 2001.
[18] A. Kurganov and E. Tadmor. New high-resolution semi-discrete central schemes for Hamilton-Jacobi equations. *J. Comput. Phys.*, 160(2):720–742, 2000.
[19] O. Lepsky, C. Hu, and C.-W. Shu. Analysis of the discontinuous Galerkin method for Hamilton-Jacobi equations. In *Proceedings of the Fourth International Conference on Spectral and High Order Methods (ICOSAHOM 1998) (Herzliya)*, volume 33, pages 423–434, 2000.
[20] C.-T. Lin and E. Tadmor. High-resolution nonoscillatory central schemes for Hamilton-Jacobi equations. *SIAM J. Sci. Comput.*, 21(6):2163–2186 (electronic), 2000.
[21] H. Liu, S. Osher, and R. Tsai. Multi-valued solution and level set methods in computational high frequency wave propagation. *Commun. Comput. Phys.*, 1:765–804, 2006.
[22] X.-D. Liu, S. Osher, and T. Chan. Weighted essentially non-oscillatory schemes. *J. Comput. Phys.*, 115(1):200–212, 1994.
[23] S. Osher. Riemann solvers, the entropy condition, and difference approximations. *SIAM J. Numer. Anal.*, 21(2):217–235, 1984.
[24] S. Osher and C.-W. Shu. High-order essentially nonoscillatory schemes for Hamilton-Jacobi equations. *SIAM J. Numer. Anal.*, 28(4):907–922, 1991.
[25] C.-W. Shu. Essentially non-oscillatory and weighted essentially non-oscillatory schemes for hyperbolic conservation laws. In *Advanced numerical approximation of nonlinear hyperbolic equations (Cetraro, 1997)*, volume 1697 of *Lecture Notes in Math.*, pages 325–432. Springer, Berlin, 1998.
[26] C.-W. Shu. High order ENO and WENO schemes for computational fluid dynamics. In *High-order methods for computational physics*, volume 9 of *Lect. Notes Comput. Sci. Eng.*, pages 439–582. Springer, Berlin, 1999.
[27] C.-W. Shu and S. Osher. Efficient implementation of essentially nonoscillatory shock-capturing schemes. *J. Comput. Phys.*, 77(2):439–471, 1988.
[28] C.-W. Shu and S. Osher. Efficient implementation of essentially nonoscillatory shock-capturing schemes. II. *J. Comput. Phys.*, 83(1):32–78, 1989.
[29] E. F. Toro. *Riemann solvers and numerical methods for fluid dynamics*. Springer-Verlag, Berlin, second edition, 1999. A practical introduction.

Iowa State University, Mathematics Department, Ames, IA 50011
E-mail address: haseena@iastate.edu; hliu@iastate.edu